CLIMATOLOGY

Speleothem record of mild and wet mid-Pleistocene climate in northeast Greenland

G. E. Moseley[1]*, R. L. Edwards[2], N. S. Lord[3,4], C. Spötl[1], H. Cheng[5,6,7]

The five interglacials before the Mid-Brunhes Event (MBE) [c.430 thousand years (ka) ago] are generally considered to be globally cooler than those post-MBE. Inhomogeneities exist regionally, however, which suggest that the Arctic was warmer than present during Marine Isotope Stage (MIS) 15a. Using the first speleothem record for the High Arctic, we investigate the climatic response of northeast Greenland between c.588 and c.549 ka ago. Our results indicate an enhanced warmth of at least +3.5°C relative to the present, leading to permafrost thaw and increased precipitation. We find that $\delta^{18}O$ of precipitation was at least 3‰ higher than today and recognize two local cooling events (c.571 and c.594 ka ago) thought to be caused by freshwater forcing. Our results are important for improving understanding of the regional climatic response leading up to the MBE and specifically provide insights into the climatic response of a warmer Arctic.

INTRODUCTION

The five interglacial periods before the Mid-Brunhes Event (MBE), which occurred between Marine Isotope Stages (MIS) 13 and 11, are generally considered to be globally cooler than those post-MBE (*1*–*7*). In contrast to this global overview, modeling (*3*) and proxy evidence (*8*–*11*) exist at regional scales indicating warmer-than-present climates before the MBE, particularly in the northern mid- and high latitudes, and especially during MIS 15a. MIS 15a, in itself, is of further interest because of its close orbital similarity to the last interglacial MIS 5e (*3*), which is often used as a baseline in climate studies for a past warmer-than-present climate. Despite the high summer insolation associated with MIS 15a, atmospheric greenhouse gas concentrations (*12*–*15*) were relatively low for an interglacial, thus mitigating the effects of the extra warmth (*2*, *3*) provided by insolation, leading to a globally cool climate. Efforts to understand the contribution of CO_2 and insolation to interglacial climates showed that despite MIS 15a being globally relatively cool compared to post-MBE interglacials, the regional response was very different, with anomalously high temperatures shown for the Arctic during both summer and winter seasons (*3*). The regional climatic disparities and their relationship to the global climate leading up to the MBE are poorly understood because of a lack of well-dated paleoclimate records that exist to test these models. Furthermore, given that the Arctic is warming at more than twice the rate of the global average, with temperatures now at their highest since instrumental records began (*16*), understanding more about how the Arctic responds in a warmer world is of utmost importance. The warm Arctic climate associated with MIS 15a thus potentially offers an important analog for improving our understanding of how the Arctic responds in a warmer world.

Here, we investigate the pre-MBE climate in the High Arctic, specifically during the period MIS 15a-14, using the first speleothem record for Greenland. The record is from the highly sensitive northeast Greenland (*17*–*20*), located far from the deep ice cores (Fig. 1) in an ice-free area characterized by extensive deep permafrost. The growth interval of the speleothem provides important constraints on the timing of permafrost thaw related to a locally warmer-than-present climate and enhanced atmospheric hydrological regime. These findings thus confirm modeling results showing that the climate of the Arctic was milder and wetter than today during MIS 15a, despite a globally cool climate, and that warmth continued into the "missing glacial" MIS 14.

Greenland caves and speleothems

Solution caves located in Silurian limestones of northeast Greenland (*21*) (80.38°N, 21.74°E) were first reported in 1960 (Fig. 1) (*22*). The largely horizontal caves are situated at distinct elevations between c.350 and 670 m above sea level (a.s.l.) in a 1-km-long, north-south trending tributary valley of the larger Grottedal valley (Figs. 1 and 2) (*22*, *23*). The caves reach a maximum of 12 m wide, 100 m long and are all blocked by ice or cave fill. In 1960, the presence of one 10-cm-thick, coarsely crystalline calcite flowstone was reported (520 m a.s.l.) (*22*).

The caves are located c.35 km from the coast and c.60 km from the Greenland Ice Sheet (GrIS) margin. Today, the region is arid, with an annual precipitation of c.200 mm (*24*). In the cave region, 50% of the annual precipitation presently occurs on 16 days of the year, with May–June being the driest months and September being the wettest month, although in reality there is limited monthly variability (c.0.35 to 0.81 mm day^{-1}) (*24*). Winter precipitation sources are centered over the northern (>45°N) North Atlantic and, in particular, the Norwegian Sea. These sources remain in summer but are diminished as a greater contribution is derived from local land and ocean sources (*24*). The nearest weather stations are situated on the GrIS c.70 km (370 m a.s.l.) and 90 km (870 m a.s.l.) to the southwest of the caves. They recorded a mean annual surface air temperature (MAAT) of −13.2° and −18.4°C, respectively, for the period July 2008 to September 2018 (*25*). Further afield, MAAT on the coast at Station Nord (180 km north) and Danmarkshavn (400 km south) is c.−18° and −11°C, respectively (*26*). In contrast, the climate of Grottedal is more continental and warmer during the summer as compared to either the GrIS or coastal stations (*27*). The Grottedal land area is snow-free during the summer, although the plateau

[1]Institute of Geology, University of Innsbruck, Innrain 52, 6020 Innsbruck, Austria. [2]Isotope Geochemistry Laboratory, School of Earth and Environmental Sciences, University of Minnesota, John T. Tate Hall, 116 Church Street SE, Minneapolis, MN 55455, USA. [3]Cabot Institute for the Environment, University of Bristol, Bristol, UK. [4]School of Geographical Sciences, University of Bristol, Bristol, UK. [5]Institute of Global Environmental Change, Xi'an Jiaotong University, Xi'an 710054, China. [6]State Key Laboratory of Loess and Quaternary Geology, Institute of Earth Environment, Chinese Academy of Sciences, Xi'an 710061, China. [7]Key Laboratory of Karst Dynamics, MLR, Institute of Karst Geology, CAGS, Guilin 541004, China.
*Corresponding author. Email: gina.moseley@uibk.ac.at

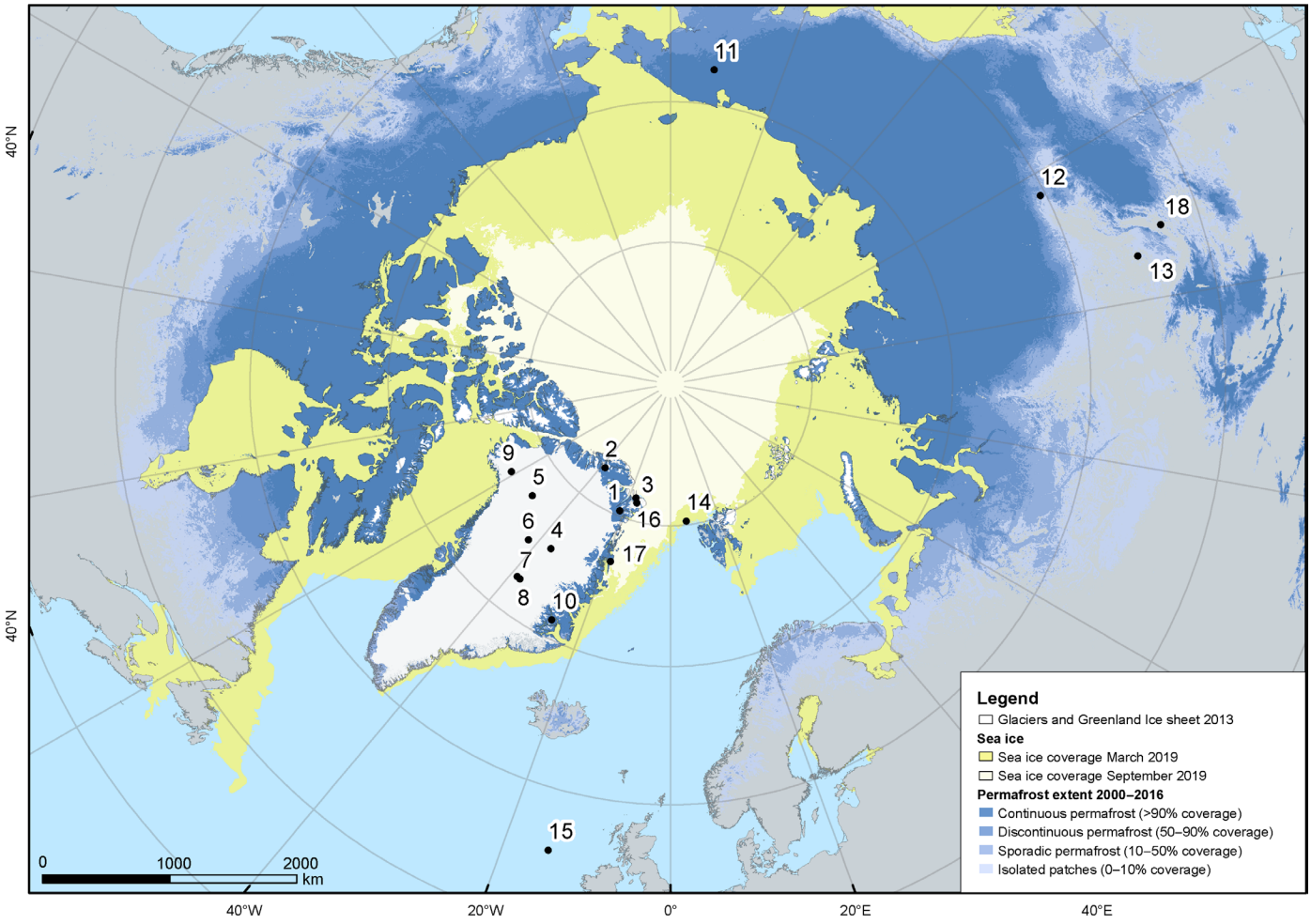

Fig. 1. Greenland cave study area compared to other sites discussed in text and sites of importance. 1: Grottedal caves site (this study); 2 to 10: Sites of ice core drilling (2: Hans Tausen ice cap; 3: Flade Isblink ice cap; 4: East Greenland Ice-core Project (EastGRIP); 5: North Greenland Eemian Ice Drilling (NEEM); 6: North Greenland Ice Core Project (NGRIP); 7: Greenland Ice Core Project (GRIP); 8: Greenland Ice Sheet Project 2 (GISP2); 9: Camp Century; 10: Renland ice cap); 11: Lake El'gygytgyn; 12: Lenskaya Cave; 13: Botovskaya Cave; 14: Ocean Drilling Programme (ODP) 910; 15: ODP 980; 16: Station Nord; 17: Danmarkshavn; 18: Lake Baikal. Figure 1 is constructed from the following datasets: GrIS (*69*), sea ice extent (*70*), permafrost (*71*), and countries (*72*).

above the caves (740 m a.s.l.) has previously hosted a small ice cap (*22*), which is now gone. Patterned ground (fig. S1) containing permafrost and deep ice-wedge depressions exists in the region. Given the contemporary arid climate and frozen ground, as well as an environment largely devoid of soil and vegetation, the modern environmental conditions severely limit karstification and preclude deposition of speleothems, as supported by the absence of drips within the caves and the extensive presence of hoar frost indicating cave air temperatures below freezing. The presence of flowstone thus indicates milder and wetter conditions in the recent geological past.

A 12-cm-thick sample of the flowstone (GD8-1; fig. S2) (*22*) was collected from a short cave during an exploratory expedition in 2015. For preservation and logistical reasons, the collected sample was not in situ, although a large portion of the sequence was in situ or close to it; thus, it is not expected that GD8-1 traveled far from its original position.

The sampled cave is not officially named by the Greenlandic authorities; hence, it is simply referred to here as GD8, which reflects the cave code it was given during the 2015 Greenland Caves Project (GCP) expedition (*28*). GD8 cave is 11 m long by 4 m wide by 4 m high (fig. S2). It contains speleogenetic features typical of a phreatic-vadose karst cave including anastomoses on the ceiling, three distinct wall notches indicating former water-table elevations, and scallops that indicate that the direction of flow was away from the present-day entrance and into the cave (*23*, *28*). Similar to all other caves explored in this region, GD8 opens in a steep cliff of the tributary valley, which is formed by fluvioglacial erosion, locally exposing flowstone deposits at the surface. Today's cave size and morphology as well as the abundance of frost shattering are therefore vastly different from the conditions when the flowstone was deposited. Because of the short length, modern cave air temperature measurements for GD8 offer limited information, as they would simply reflect the weather conditions external to the cave at a given point in time. Some useful information may, however, be obtained from another cave at a similar elevation within the same valley. At 95 m long, U-Tut Ilusilik Qaarusussuaq (U-shaped cave) is the longest cave discovered in this area (*23*). It is relatively horizontal, "U-like" in shape, and has two entrances that open at an elevation of c.530 m a.s.l. (i.e., at a comparable elevation to GD8 at c.520 m a.s.l.). The middle of the cave, c.48 m from the entrance and found in the

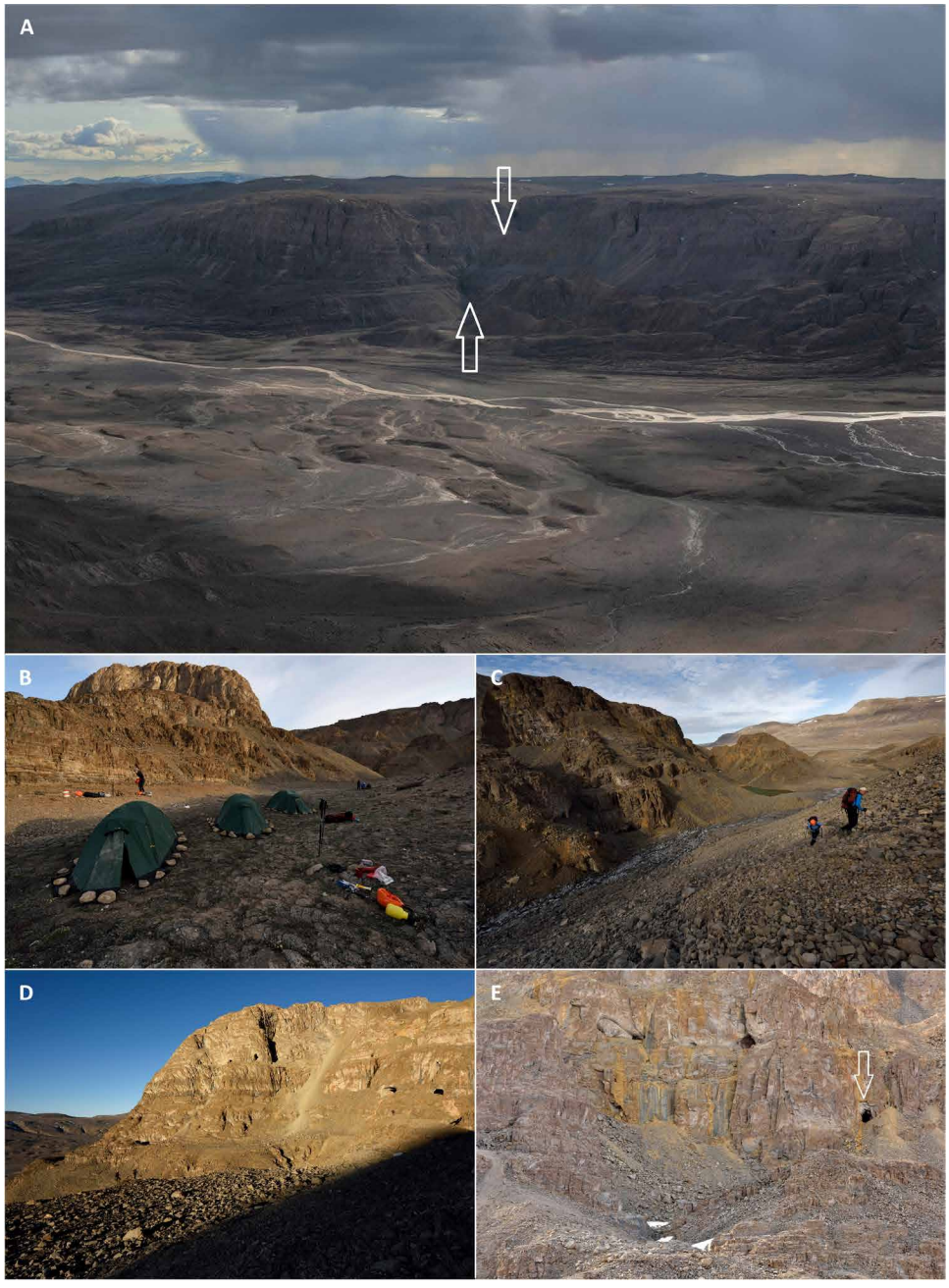

Fig. 2. Grottedal and the cave-bearing tributary valley. (**A**) View looking south across Grottedal at the tributary valley containing the caves. Arrows highlight the location of the cave-bearing tributary valley. (**B** and **C**) Tributary valley containing the caves. (**D**) Cave entrances on the eastern wall of the tributary valley with Grottedal in the background. (**E**) View of three cave entrances in the west wall. The cave sampled in this study is highlighted with an arrow. Photos: Robbie Shone (@shonephotography).

trough of the "U," is found within the twilight zone and in a location where external air temperatures begin to have a reduced effect on the cave air temperature. Here, a spot temperature measurement of −3.5°C was taken on 6 July 2019. Another horizontal cave within the same area, Inussuk Innartooq Qaarusussuaq (Cairn Climb Cave), located at 540 m a.s.l., but only 19 m in length, also had a comparable air temperature of −3.3°C, c.10 m from the entrance (*23*) on 7 July 2019. Elsewhere within the wider region, much colder cave air temperatures of −6° to −17°C have also been recorded, but these are found in caves of higher elevation (up to 825 m a.s.l.) or in gently dipping caves (*23*) that display cold air-trap characteristics (*29*, *30*). Given that GD8 is truncated and only a relic of the system it was when the flowstone was deposited, it is not possible to say whether it was morphologically horizontal or dipping.

RESULTS

U-Th dating combined with age modeling (figs. S3 and S4 and table S1) indicates that the flowstone was deposited between c.588 and c.537 thousand years (ka) ago. Isotopic measurements are precise despite low

U concentrations (tens of parts per billion), and corrections for initial Th are negligible. Because the age of the sample is near the limit of the U-Th dating method, uncertainties in age are larger than would be the case for younger samples. Nevertheless, all ages are stratigraphically in order within uncertainty, consistent with closed-system evolution, while two separate slabs taken from the sample yield reproducible results (fig. S4). $\delta^{18}O$ and $\delta^{13}C$ of the speleothem calcite range between c.−11 to −16‰$_{\text{Vienna Pee Dee Belemnite (VPDB)}}$ and +2 to −6‰$_{\text{VPDB}}$, respectively, and correlation between $\delta^{18}O$ and $\delta^{13}C$ is minimal (fig. S5), suggesting limited kinetic isotope fractionation (*31*).

DISCUSSION

Results of the U-Th–based age modeling indicate that deposition occurred through MIS 15a and into MIS 14 (Fig. 3A), although it is entirely plausible that growth was not continuous and may have had a stop-start character related, for instance, to the seasonal cycle or extended cold periods on decadal or centennial scales superimposed on a general period of warmth. One might also consider that there may be unidentified hiatuses and that deposition may have occurred during MIS 13; however, the youngest U-Th age from slab 2 indicates that this was not the case (fig. S3). It is also reasonable to question whether or not the speleothem was deposited during a warmer and wetter climate, or possibly beneath a warm-based ice cap. Until recently, a small ice cap was present on the plateau above the caves (*22*), but despite this, no active drips were reported within the caves, and they remained frozen with air temperatures below 0°C (*23*). Conditions may have been different in the distant past, but these modern observations indicate that the caves remained in the permafrost when an ice cap was present above. Furthermore, despite

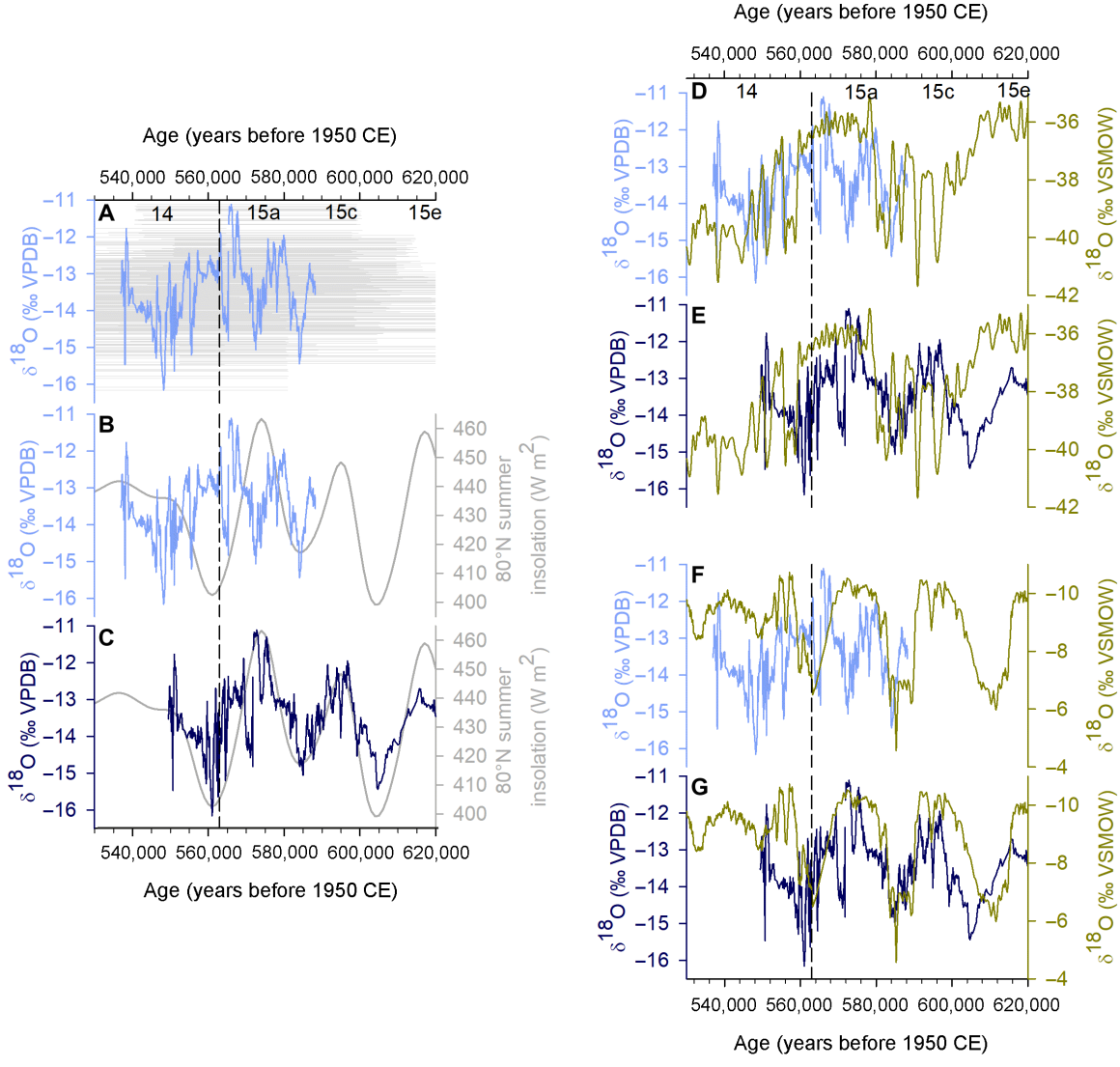

Fig. 3. Orbital refinement of U-Th–based age model. (**A**) Original U-Th–based StalAge age model including 2σ uncertainty (horizontal gray bars). (**B**) U-Th–based age model (light blue) relative to 80°N summer insolation (gray) (*32*). (**C**) U-Th–based age model (dark blue) tuned to 80°N summer insolation (gray) (*32*). (**D**) U-Th–based age model (light blue) relative to Greenland synthetic $\delta^{18}O$ record (dark yellow) (*34*). (**E**) Orbitally-refined age model (dark blue) relative to Greenland synthetic $\delta^{18}O$ record (dark yellow) (*34*). (**F**) U-Th–based age model (light blue) relative to composite Asian monsoon $\delta^{18}O$ record (dark yellow) (*33*). (**G**) Orbitally refined age model (dark blue) relative to composite Asian monsoon $\delta^{18}O$ record (dark yellow) (*33*). Vertical dashed lines indicate MIS 15a-14 boundary. CE, common era.

extensive searching, no late Holocene speleothems have been found, which would indicate deposition beneath a warm-based ice cap. Lack of an ice cap, specifically during the MIS 14 period, is also supported by the $\delta^{13}C$ profile, which indicates development of a soil at this time (fig. S4). We therefore consider a warmer and wetter climate to be a more probable climate state for the deposition of the speleothem.

The pattern of the $\delta^{18}O$ variability yielded by this age model does not exhibit a particularly strong correlation to orbital parameters (Fig. 3B). It is possible, however, to refine the age model within the limits of uncertainties and tune it to 80°N insolation (Fig. 3C) (*32*). The orbitally refined age model suggests that speleothem deposition occurred between c.622 and c.549 ka ago, i.e., beginning at the start of MIS 15 and ending shortly within MIS 14 (Fig. 3). Naturally, the consequence of this orbital tuning is a better agreement with the $\delta^{18}O$ variability in the Asian monsoon composite speleothem record (*33*) whereby higher $\delta^{18}O$ in Greenland corresponds to lower $\delta^{18}O$ in Asia and vice versa (Fig. 3G). In contrast, comparison of the U-Th–only age model and the orbitally refined age model with the synthetic Greenland $\delta^{18}O$ record (*34*) shows that both approaches yield $\delta^{18}O$ records that are similar in timing and pattern to the Greenland synthetic curve (Fig. 3, D and E). One might even argue that millennial-scale events in the Greenland synthetic record are better correlated with the U-Th–only age model (Fig. 3D). At present, we do not adopt either age model as the best approach because many questions remain open with regard to the relationship between Greenland 80°N speleothem $\delta^{18}O$ and 80°N summer insolation. Furthermore, the efficacy of orbital tuning for this particular time period has been shown to be ineffective (*35*). The remainder of the discussion surrounding the speleothem growth interval will therefore be based around the period c.588 to c.549 ka ago, which is where the two age models overlap.

Regardless of the age model adopted, the speleothem growth interval indicates a warmer and wetter climate as compared to today in northeast Greenland (80°N) during the period of high-amplitude insolation changes leading up to the MBE (Fig. 4). Speleothem deposition was active during MIS 15a to MIS 14, although if the orbitally refined age model is taken into consideration, then deposition may have begun earlier in MIS 15e (Fig. 3C). This period of high-amplitude precessional fluctuations was modulated by the high eccentricity that occurred at the time (*35*); consequently, the MIS 15a interglacial (*1*) had the third highest Northern Hemisphere summer insolation maximum of the past million years (fig. S6) (*32*), an effect that was further compounded at high latitudes by the high obliquity. MIS 15c and the interglacial MIS 15e also experienced relatively high insolation maxima (fig. S6) (*32*), with MIS 15e generally considered to be of comparable strength to MIS 15a in most records (*1*).

Both modeling and proxy records indicate that the five interglacial climates before the MBE were generally cooler annually and seasonally on global and hemispheric scales than those post-MBE. The only exception to this is the MIS 15a summer temperature, which models suggest were warmer than present globally and hemispherically, with the Northern Hemisphere summer being the warmest of the past nine interglacials (*2*, *3*). The relatively "cool" annual global climate of MIS 15a is considered to be a consequence of low greenhouse gas concentrations (Fig. 4L) mitigating the effects of high summer insolation (*2*, *3*). The speleothem record presented here, however, provides (the first) radiometrically dated evidence for a warmer and wetter MIS 15a climate in the High Arctic. Further evidence for MIS 15a being a warm interglacial, especially in the high northern latitudes, is further provided by U-series–dated speleothem growth periods in eastern Siberia at 60°N, which indicate permafrost absence (Fig. 4G) (*36*). At this time, the orbitally tuned Lake El'gygytgyn (67.5°N) sediment cores also show an increase in planktonic concentration and diversity (Fig. 4F) (*10*), whereas Lake Baikal (53°N) diatom productivity was also very high (Fig. 4I) (*9*). In the case of Lake El'gygytgyn and Lake Baikal, these increased levels of productivity also partly continue into MIS 14, similar to our speleothem growth period. In contrast, pollen records from south Greenland, which are used as an indicator of reduced ice volume, are not particularly responsive at this time in comparison to other interglacials, although they are approximately 3.5 times higher than for the Holocene (Fig. 4H) (*37*), indicating a greater ice-free area than is found at present. MIS 9e, which is shown in some records to be one of the warmest interglacials of the past 800,000 years (*1*), also does not show a particularly strong pollen response in this record (Fig. 4H), although, in contrast, sea surface temperature (SST) records from a nearby core indicate that MIS 9e was the warmest of the previous four interglacials with summer SST 3.3°C above modern values and a reduced size of the GrIS (*38*). By inference, we therefore would not necessarily expect to see a pollen response in south Greenland for MIS 15a.

Elevated MIS 15a temperatures within the High Arctic, leading to permafrost thawing, an enhanced hydrological cycle, incipient soil development, karstification, and local deposition of speleothems, were likely forced by the high summer insolation, which models show to be the dominant factor controlling interglacial temperature at high Northern Hemisphere latitudes (*3*). In the Arctic, high MIS 15a obliquity resulted in further enhancement of summer solar radiation in comparison to the rest of the planet. Warm intense summers in the Arctic subsequently led to the "summer remnant effect" (*3*) whereby summer ocean warming enhanced melting of sea ice and increased warming in the upper ocean, thus delaying formation of sea ice and reducing its thickness and thermal insulation effects the following winter. Consequently, heat was lost from the ocean to the atmosphere in early winter, resulting in an increase in winter atmospheric temperatures, specifically in the Arctic during MIS 15a, despite the low winter insolation (*3*). The increased temperature from insolation in the summer and increased temperature from the summer remnant effect in the winter thus provide a mechanism by which both summer and winter temperatures were increased, raising MAAT and leading to permafrost thawing in northeast Greenland. The lack of Arctic sea ice during MIS 15a, which is highly important for increasing temperature in the winter months (*3*), is also supported by proxy data from cores in the Arctic (Fig. 4E) (*39*), although these point to an extended sea ice–free period before the MBE and not one directly as a result of high insolation. The deposition of speleothem at 80°N in northeast Greenland, which requires a higher MAAT than at present to thaw the permafrost, thus supports model results that show Arctic MIS 15a summer, and winter temperatures were higher than at present (although annually globally they were cooler).

In addition to the increased temperature, an increase in precipitation must have also occurred in this presently arid region. Correlation between atmospheric dust records from Greenland and Antarctica is considered by some to reflect the state of the global hydrological cycle and global atmosphere (*35*). In comparison to the present, atmospheric dust content in Antarctica was lower during MIS 15a (Fig. 4D) (*40*), thus suggesting an enhanced global hydrological

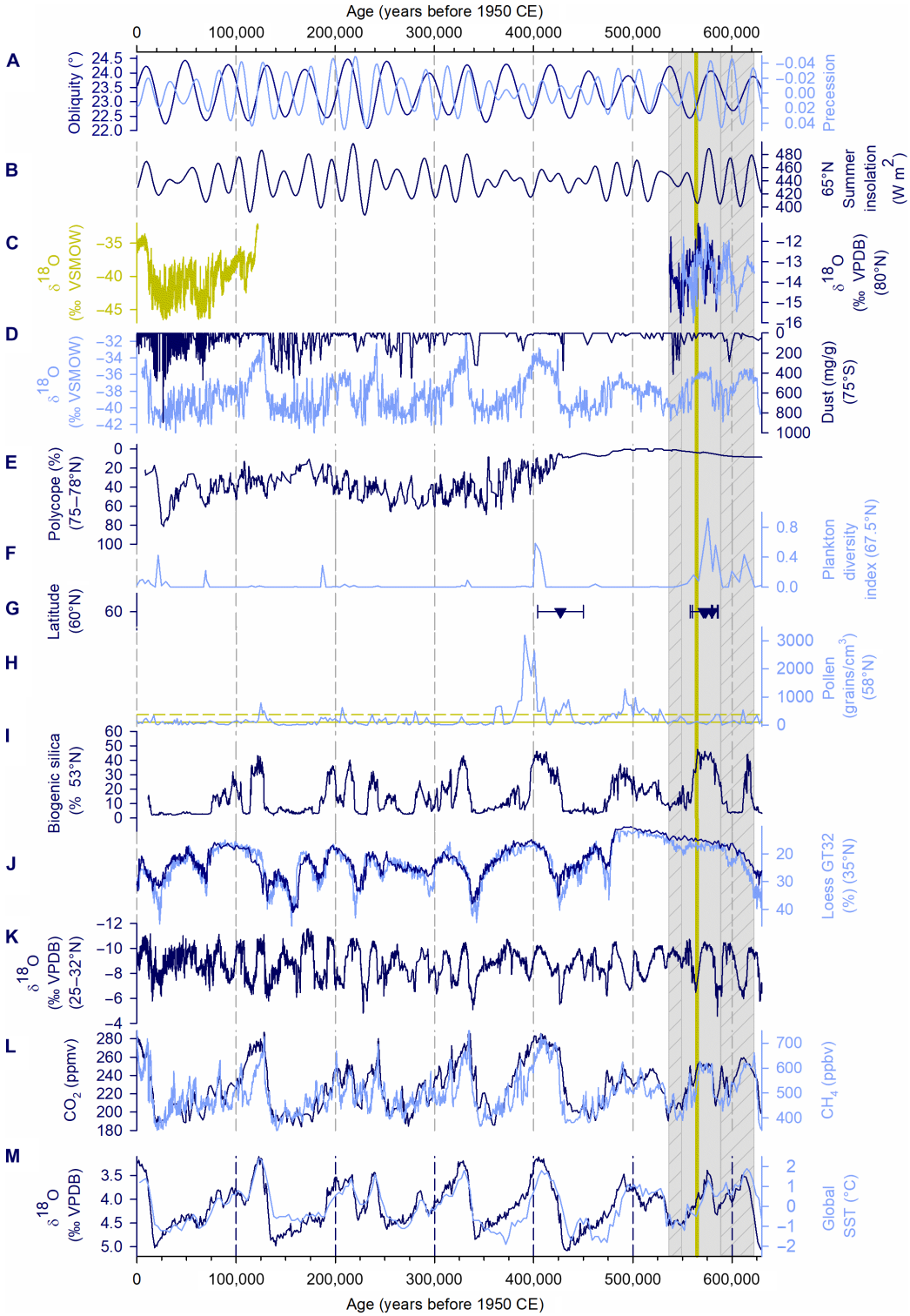

Fig. 4. Greenland speleothem δ^{18}O record compared with other paleoclimate archives for the period 0 to 630 ka ago. (**A**) Obliquity (dark blue) (*73*) and precession (light blue) (*73*). (**B**) The 65°N summer insolation (*73*). (**C**) NGRIP Greenland δ^{18}O record (dark yellow) (*74*). U-Th–based (dark blue) and orbitally refined (light blue) age models for 80.2°N Greenland speleothem δ^{18}O record (this study). (**D**) Synthetic Greenland δ^{18}O record (light blue) (*34*). EPICA Dome C (EDC) atmospheric dust (dark blue) (*40*). (**E**) Arctic Ocean *Polycope* abundance (*39*). (**F**) Lake El'gygytgyn plankton diversity index (*10*). (**G**) Eastern Siberian speleothem ages (*36*). (**H**) South Greenland marine pollen record (*37*). Solid yellow horizontal bar indicates Holocene baseline. Dashed yellow horizontal bar indicates MIS 15a baseline. (**I**) Lake Baikal biogenic silica record (*9*). (**J**) Chinese loess grain size >32 μm: Yimaguan (light blue) and Luochuan (dark blue) (*43*). (**K**) Asian monsoon composite speleothem record (*33*). (**L**) Atmospheric CO_2 (dark blue) (*12–14*) and CH_4 (light blue) (*12*, *13*, *15*) concentrations. (**M**) Global benthic δ^{18}O stack (dark blue) (*41*). Stacked global SST record (light blue) (*44*). Vertical gray bar highlights area of overlapping speleothem age models, with hatched vertical bars indicating only single age models. Vertical yellow line marks MIS 15a-14 boundary.

cycle at this time. In agreement, models indicate the largest increase in Northern Hemisphere summer monsoon precipitation during MIS 15a over the past 800 ka controlled by precessional effects at low latitudes (*3*). The moisture needed for the enhanced hydrological regime in the Arctic, which would have been needed for the speleothem growth, was likely sourced, in part, from an increase in long-range transport but more dominantly from the local ice-free open ocean, as has been predicted for a future warmer Arctic (*19*). Even under present conditions, moisture sources switch from long-range transport in the winter months to local ice-free waters and continental recycling in the summer months (*24*). It is thus expected that during MIS 15a, higher temperatures and a greater ice-free local ocean would have resulted in a higher contribution of moisture from local sources.

The continued speleothem deposition into MIS 14 is perhaps more perplexing than the growth during MIS 15a. MIS 14 is, however, considered a "missing glaciation," suggested to be a consequence of the preceding high-amplitude Northern Hemisphere insolation changes that would have mitigated glacial inception and prevented substantial ice expansion in the Northern Hemisphere (*35*). This is indicated by a lack of terrestrial evidence for Northern Hemisphere glacial expansion and is also reflected in the marine record, which displays the lowest benthic foraminifera $\delta^{18}O$ of the past 10 cold stages (Fig. 4M) (*35*, *41*), indicating lower global ice volume. Sea levels during MIS 14 were also relatively high (−67 m) (*42*), and perennial Arctic sea ice remained absent (Fig. 4E) (*39*). For the period that is coincident with the speleothem deposition, benthic foraminifera $\delta^{18}O$ were increasing and had not yet reached their maximum (*41*), pollen assemblages in south Greenland remained as high or higher than the Holocene (Fig. 4H) (*37*), and Lake El'gygytgyn was marginally productive (Fig. 4F) (*10*), whereas Lake Baikal became increasingly less productive (Fig. 4I) (*9*), Chinese loess remained at similar levels to MIS 15a (Fig. 4J) (*43*), and atmospheric dust concentrations remained relatively subdued (Fig. 4D) (*40*). Atmospheric CO_2 concentrations gradually declined over this period but showed a short sharp increase centered at c.558 ka ago (Fig. 4L) (*12*–*14*). In contrast, global SSTs in MIS 14 were as cold as during some full glacials (Fig. 4M) (*44*). A disparity therefore exists between the terrestrial records for MIS 14 and global SSTs.

Cores from the subpolar north Atlantic show that following benthic $\delta^{18}O$ changes indicating the inception into MIS 14 (Fig. 5G), ice-rafted debris events remained largely absent (Fig. 5, D and F) (*45*), polar *Neoloboquadrina pachyderma* (s) planktonic foraminifera stayed close to interglacial levels (Fig. 5, D and F) (*45*), and SSTs stayed elevated for some 14 ka (Fig. 5, E and G) (*45*, *46*). North Atlantic Deep Water production also remained active (Fig. 5E) (*46*). Continued growth of the speleothem in northeast Greenland into MIS 14 also corresponds with the timing of this "lagging warmth" (*45*) observed in the subpolar north Atlantic, although some debate exists as to whether lagging warmth was spatially limited to the east North Atlantic (*46*). It is proposed that the continued warmth during glacial inceptions in the eastern North Atlantic allowed the North Atlantic Current to remain active, transporting heat and moisture toward the Norwegian and Greenland Seas and maintaining deep-water formation (*45*). Ocean circulation may have thus continued to have an impact on the local climate in northeast Greenland at the beginning of MIS 14 enabling deposition of speleothem growth.

To further investigate the temperature and precipitation anomalies at the cave site in comparison to present-day values, a climate emulator (*47*) was forced at 1-ka resolution. Temperature and precipitation peaks occurred during MIS 15a, between c.580 and c.565 ka ago (Fig. 6), both at the study site grid box and in several of the surrounding grid boxes (Fig. 7). While the emulator was successful in capturing these peaks, the modeled maximum temperature and precipitation were +2.6°C and +3.0 mm $month^{-1}$ above preindustrial values.

As mentioned, present-day cave air temperatures as recorded during the summer are c.−3.5°C. First, in the absence of a local meteorological station, it is not possible to say whether this is comparable to MAAT. Other similar short caves located within the Arctic tend to record summer cave air temperatures above MAAT (*48*), and we suspect that this is also the case for the short caves studied here in northeast Greenland. The nearest weather station, located c.70 km to the southwest of the caves at the base of the GrIS, recorded a MAAT of −13.2°C for the period July 2008 to September 2018 (*25*). Given the close proximity to the GrIS, the MAAT at the weather station is likely to be lower than at the cave site. The true MAAT at the cave site today therefore likely lies between −3.5° and −13.2°C. We must also consider that the truncated cave morphology as observed today is not representative of the untruncated, longer cave system that would have existed during MIS 15a, which, being less exposed to short-term exchange with the surface, would have likely had a more stable air temperature and possibly one that was closer to MAAT. Taking the present-day cave air temperature of −3.5°C as a maximum present-day MAAT, MIS 15a MAAT must have been at least 3.5°C higher than today (and likely more) to raise cave air temperatures above freezing, which would have implications for reducing the size of the GrIS (*38*). The emulator thus does not capture the warmth needed to achieve these temperature anomalies. Furthermore, the emulator results for MIS 15a are comparable to the results for MIS 5e (+2.5°C and +3.8 mm $month^{-1}$), which is substantially less than the estimated anomaly of +8° ± 4°C or +7° to +11°C (*49*, *50*) for the North Greenland Eemian Ice Drilling (NEEM) site on the ice sheet.

A full discussion of the limitations of the emulator is provided elsewhere (*47*), but one that is relevant here is that the General Circulation Model (GCM) simulations with varying ice sheets (*51*) use the ICE-5G ice sheet reconstructions (*52*), which are based on paleo-data (global sea level and/or ice sheet extent) since the Last Glacial Maximum (LGM). The emulator therefore assumes that previous glacial and interglacial episodes are similar to the LGM and Holocene, respectively, which is known not to be the case. However, for glaciations that occurred before the last glacial cycle, there is very little or no paleo-data available that would enable the three-dimensional reconstructions of the ice sheets that are required here. Differences in the height, topography, and/or extent of the ice sheets during MIS 15a may have an impact on the simulated climate, e.g., through changes in atmospheric circulation or North Atlantic storm tracks. In addition, the emulator models mean annual climate, but it may be that greater warming is experienced during a particular season, with, e.g., possible implications for sea ice and associated feedbacks.

It should be noted that this speleothem $\delta^{18}O$ record provides a first approximation of the Greenland atmospheric $\delta^{18}O$ signal for a period beyond the limit of the Greenland ice cores (Fig. 4C). Accounting for the differences in Vienna Standard Mean Ocean Water (VSMOW) versus VPDB, $\delta^{18}O$ values are offset between the cave site (c.−11 to −16‰$_{VPDB}$) and the interior of the ice sheet (c.−32 to −46‰$_{VSMOW}$), with the much higher values at the cave site being due to the warmer climate regime

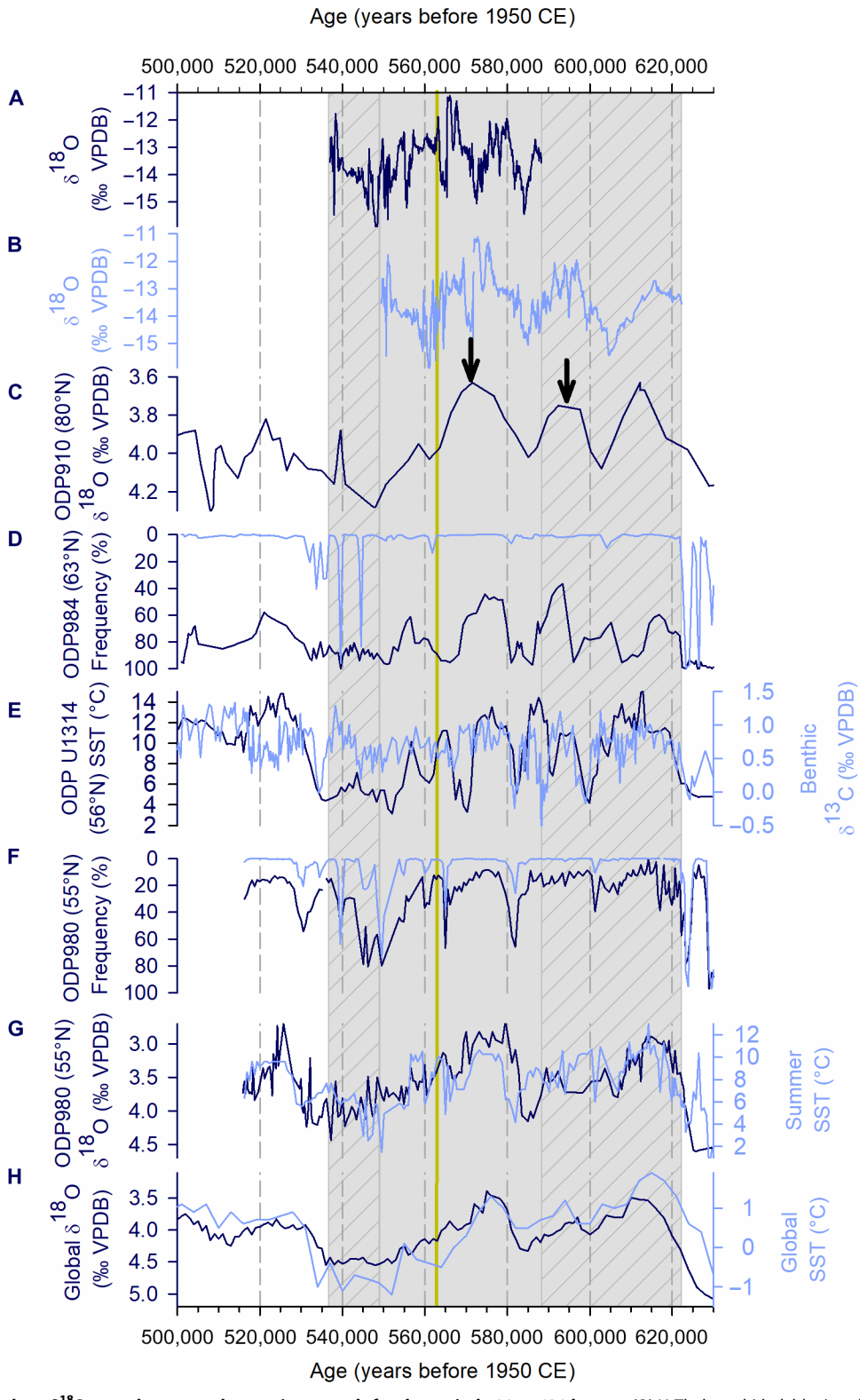

Fig. 5. Greenland speleothem $\delta^{18}O$ record compared to marine records for the period 500 to 630 ka ago. (**A**) U-Th–based (dark blue) and (**B**) orbitally refined (light blue) age models for 80.2°N Greenland speleothem $\delta^{18}O$ record (this study). (**C**) ODP 910 80°N Arctic Gateway $\delta^{18}O$ planktic foraminifera record. Arrows indicate freshwater pulses (*59*). (**D**) ODP 984 63°N ice-rafted debris (light blue) and *N. pachyderma* (s.) abundance (dark blue) (*45*). (**E**) ODP U1314 56°N SST (dark blue) and benthic $\delta^{13}C$ (light blue) (*46*). (**F**) ODP 980 55°N ice-rafted debris (light blue) and *N. pachyderma* (s.) abundance (dark blue) (*45*). (**G**) ODP 980 55°N benthic foraminifera $\delta^{18}O$ (dark blue). Summer SST (light blue) (*45*). (**H**) Global benthic $\delta^{18}O$ stack (dark blue) (*41*). Stacked global sea surface temperature record (light blue) (*44*). Vertical gray bar highlights the area of overlapping speleothem age models, with hatched vertical bars indicating only single age models. Vertical yellow line marks the MIS 15a-14 boundary.

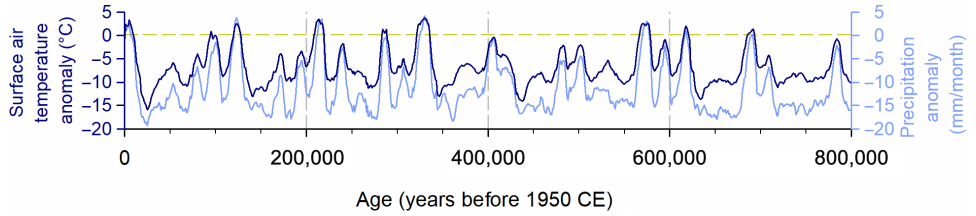

Fig. 6. Emulator results for surface air temperature anomaly and precipitation anomaly at the cave site in northeast Greenland over the period 0 to 800 ka ago. Surface air temperature anomaly (dark blue). Precipitation anomaly (light blue). Horizontal dashed line indicates preindustrial baseline.

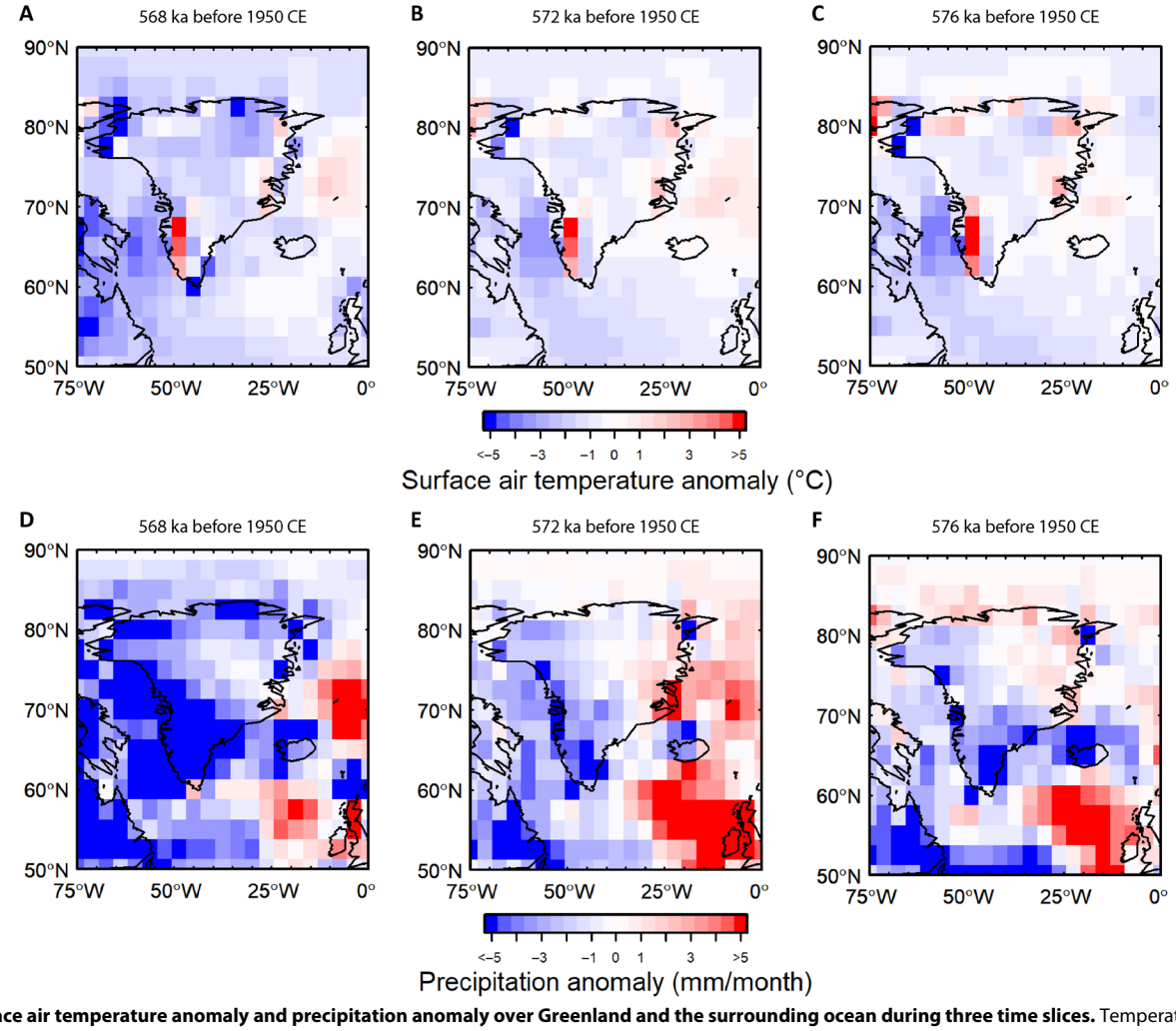

Fig. 7. Surface air temperature anomaly and precipitation anomaly over Greenland and the surrounding ocean during three time slices. Temperature anomaly: (**A**) 568 ka ago, (**B**) 572 ka ago, and (**C**) 576 ka ago. Precipitation anomaly: (**D**) 568 ka ago, (**E**) 572 ka ago, and (**F**) 576 ka ago. The cave site is shown as a black point.

under investigation, closer proximity to the source, and lower elevation. Because the glacial-interglacial isostatic range is only c.30 m (*53*), it is not expected that glacio-isostatic adjustments had a large impact on $\delta^{18}O$ of the recharge water. As a point of comparison, $\delta^{18}O$ values from the nearby Flade Isblink ice cap (81.3°N, 15.7°W, c.700 m a.s.l.) vary between −21‰$_{VSMOW}$ during the Medieval Climate Anomaly and −24‰$_{VSMOW}$ during the Little Ice Age (*54*). On the basis of the speleothem $\delta^{18}O$ values of −11 to −16‰$_{VPDB}$, we constrain the $\delta^{18}O$ range of the infiltrating water at the cave site during MIS 15a-14 as c.−14‰$_{VSMOW}$ (for −11‰$_{VPDB}$ calcite) to c.−19‰$_{VSMOW}$ (for −16‰$_{VPDB}$ calcite), assuming a minimum temperature of 1°C (*55*–*57*). If temperatures were higher, then the recharge water would need to have been isotopically heavier to produce −11‰$_{VPDB}$ calcite (*55*–*57*), thus constraining these as minimum values for the infiltration water. In comparison, congelation ice today within the Grottedal caves varies from −17 to −25‰$_{VSMOW}$ (Fig. 8 and table S2), which is in agreement with an annual mean modeled $\delta^{18}O$ of precipitation of c.−20‰$_{VSMOW}$ for the site (*58*). Infiltration water with $\delta^{18}O_{VSMOW}$ at least c.3‰ heavier than today would therefore be needed to form the −11‰$_{VPDB}$ calcite. We stress, however, that 3‰$_{VSMOW}$ is the

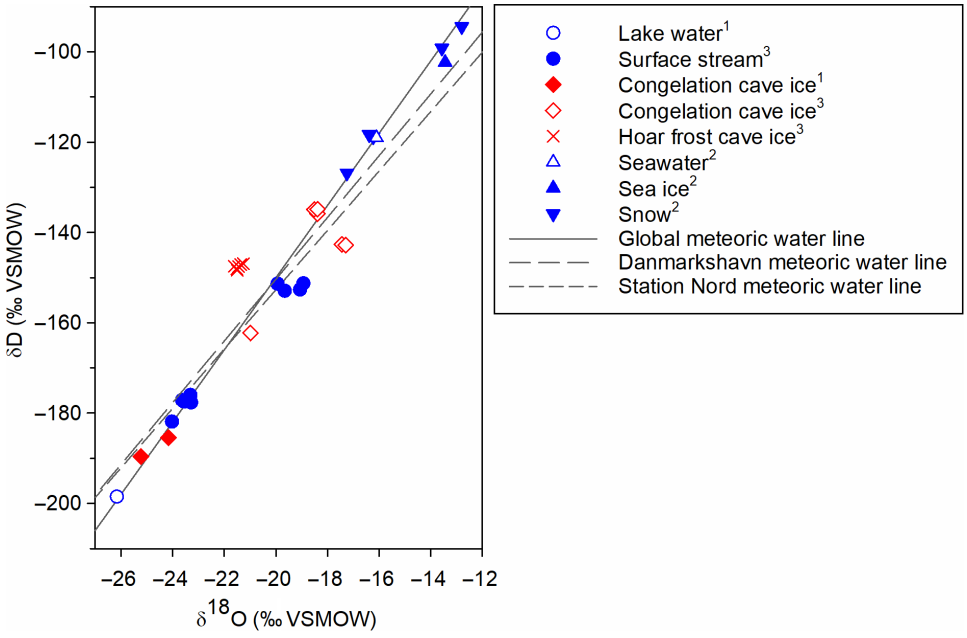

Fig. 8. Stable isotopic composition of water and ice samples relative to the global meteoric water line, Danmarkshavn meteoric water line (81.6°N) (*26*), and Station Nord meteoric water line (76.8°N) (*26*). Region and expedition: [1]2015 Grottedal/Centrumsø (80.2°N), [2]2018 Wegener Halvø (71.7°N), and [3]2019 Grottedal/Centrumsø (80.2°N).

minimum difference in comparison to today given that temperatures could have been more than 1°C, and that the range in $\delta^{18}O$ of modern precipitation extends down to −20 to −25‰. Today, the $\delta^{18}O$ temperature gradient for the region is modeled at c.0.9 to 1.3‰ $°C^{-1}$ (*58*); thus, while it is not known whether this relationship was the same during MIS 15a-14, it highlights the possibility that a MAAT change of 3.5°C could account for a c.3‰ increase in $\delta^{18}O_{VSMOW}$ of mean annual precipitation. A higher increase in $\delta^{18}O_{VSMOW}$ of precipitation could, of course, be achieved through higher temperatures or by other additional mechanisms. As mentioned, even under present conditions, moisture sources switch from long-range transport in the winter months to local ice-free waters and continental recycling in the summer months (*24*). Predictions for a future warmer Arctic indicate an increase in precipitation (*19*, *20*) and especially rain in all areas of the Arctic except the interior of the GrIS (*20*). By the end of this century, the greatest changes in Arctic precipitation are expected over the Arctic Ocean and northeast Greenland and, specifically, in the late autumn-winter months associated with evaporation from ice-free Arctic waters (*19*). In a warmer MIS 15a-14 Arctic climate in which sea ice was absent (Fig. 4E) (*39*), a much higher contribution of precipitation was likely sourced locally, thus reducing Rayleigh fractionation, leading to a further increase in $\delta^{18}O$ of precipitation. Seasonality changes may have added additional controls, but given that the increase in precipitation is expected to be more dominant in autumn-winter months (when $\delta^{18}O$ would be less than for summer months), it is thought that the temperature difference and more local moisture source were likely the main factors affecting the increased $\delta^{18}O$ of precipitation during MIS 15a-14.

Given the large uncertainties in the age model, we do not provide a full interpretation of the speleothem $\delta^{18}O$ signal but do consider the effects of two freshwater events through the Arctic Gateway (Fig. 5C) (*59*) on the local climate. The largest of these freshwater events, centered on c.571 ka ago, occurred within age-model uncertainties with a distinctive depletion in $\delta^{18}O$ in both age models (Fig. 5, A and B), making it likely that this freshwater event had a cooling effect on the local climate. Of interest here is the decoupling between the surface temperatures of the Arctic Gateway and subpolar North Atlantic, which is indicated by the depletion in planktic $\delta^{18}O$ in the Arctic Gateway (Fig. 5C) versus a continued low abundance of subpolar North Atlantic polar foraminifera (Fig. 5, D and F) and unchanged SSTs (Fig. 5, E and G). Another smaller freshwater event centered on c.594 ka ago corresponds timewise also to a small depletion in speleothem $\delta^{18}O$ in the orbitally refined age model. As for the larger freshwater event, the subpolar North Atlantic records do not respond.

In conclusion, over the past 800,000 years, the five interglacials (MIS 13a-19c) before the MBE are considered to be globally cooler than the six interglacials post-MBE (*1*). Despite this, modeling results suggest that a period of warmth, higher than at present, existed in the Arctic during MIS 15a as a result of the exceptionally high summer insolation at that time (*2*, *3*). The growth of speleothem during MIS 15a in northeast Greenland, thus requiring the percolation of precipitation into the cave and therefore a warmer and wetter climate in comparison to today, supports the modeling results and the notion that the Arctic can be anomalously warm, even during a period of relatively mild global climate. Such findings do not, at this stage, preclude speleothem deposition during other interglacials, either pre- or post-MBE, and do not limit the driving force for increased warmth to high summer insolation only. Of importance with regard to the results presented here is the novel, first Arctic speleothem record, which has been used as an important test of model results, confirming a warmer and wetter Arctic during MIS 15a and therefore regional heterogeneities with respect to the global climate state. Furthermore, the continued growth of the speleothem into MIS 14 extends the spatial influence of the lagging warmth that existed during the start of this "missing glacial" beyond the eastern North Atlantic.

The growth of speleothem during MIS 15a-14 in northeast Greenland indicating a warmer and wetter climate was associated with high Northern Hemisphere summer insolation and relatively low atmospheric greenhouse gas concentrations. These boundary conditions, which were more comparable to those for MIS 5e, are different to what is expected in the future, i.e., comparatively low Northern Hemisphere summer insolation and high greenhouse gas concentrations. Nevertheless, the results presented here further highlight the sensitivity of the Arctic and, in particular, northeast Greenland to changing boundary conditions and climate states. As is predicted for the future (*18*–*20*), warmer climate states in the past have resulted in a wetter climate for which the moisture was likely sourced more locally from an open ice-free ocean.

MATERIALS AND METHODS

U-Th dating

Sample GD8-1 was collected ex situ from GD8 cave in northeast Greenland. The sample was cut in half, and two slabs were taken as a test of reproducibility. Both slabs were polished to remove cut marks and improve the finish. Subsamples for U-Th dating were drilled using a handheld drill in a thoroughly cleaned laminar flow hood used exclusively for low U concentration carbonate samples. Because of the low uranium concentration and possibility of leaching, this method was preferred to cutting small chips and cleaning in an ultrasonic bath. Typical sample sizes were 300 mg. Extraction and purification of U and Th followed standard chemistry procedures (*60*) and were performed at the Isotope Geochemistry laboratory at the University of Minnesota. Samples were spiked with a dilute mixed ^{229}Th-^{233}U-^{236}U tracer to allow for correction of instrumental fractionation and calculation of U and Th concentrations and ratios. Measurements were conducted on a Thermo-Finnigan Neptune multi-collector inductively coupled plasma mass spectrometer (*61*).

Stable isotopes of calcite

Stable isotopes ($\delta^{18}O_{calc}$ and $\delta^{13}C_{calc}$) were micro-milled at a spatial resolution of 150 μm (slab 1) and 200 μm (slab 2). Measurements were conducted at the University of Innsbruck on a Thermo Fisher Scientific DeltaplusXL isotope ratio mass spectrometer linked to GasBench II and measured relative to the NBS19 standard. Analytical precisions of the standard are 0.08 and 0.06‰ for $\delta^{18}O_{calc}$ and $\delta^{13}C_{calc}$, respectively (1σ) (*62*).

Reproducibility

Given that a second speleothem sample was not available for reproducibility testing, we opted to slice two slabs from GD8-1 as a next-best step. Slab 1 was treated as the master slab from which the highest-resolution samples for stable isotopes and dating were taken. Slab 2 was treated as a basic test of slab 1 with lower-resolution spatial analysis. Within uncertainty, slab 2 reliably reproduces the results of slab 1 (fig. S3).

Secular equilibrium

Four samples yielding ages at or close to secular equilibrium were obtained for slab 1. Two of these were finite ages within uncertainty of the remainder of the age model. The other two yielded secular equilibrium ages within uncertainty. Higher-precision measurement uncertainties on these two samples that do not intersect secular equilibrium would still result in ages with very large uncertainties that intersect the age model.

Age model

Age models were constructed using the Monte Carlo approach in StalAge (*63*).

Climate emulator

The climate emulator (*47*) was trained using GCM snapshot simulations run using the UK Met Office Hadley Centre Climate Model (HadCM3) (*64*) with varying orbital parameters, atmospheric CO_2 concentration, and ice sheets, including a set covering the last glacial cycle (*51*). The emulator was forced at 1-ka resolution by orbital changes (*65*), a composite record of observed paleo-CO_2 (*66*), and a record of global sea level reconstructed using a one-dimensional ice sheet–climate model (*67*). The resulting series of global temperature and precipitation fields were then combined to provide a "continuous" climate simulation, and the climate at the grid box in which the cave is located, and the surrounding region, was examined.

Stable isotopes of surface precipitation

During the three expeditions of the GCP (2015 and 2019: Centrumsø/Grottedal region, 80.2°N; 2018: Wegener Halvø, 71.7°N) (*68*), surface waters and cave ice were sampled for analysis of oxygen and hydrogen isotopic composition. At present, the nearest monitoring of isotopes in precipitation takes place at Station Nord, some 180 km to the north and located on the coast. Spot sampling of surface waters and cave ice at the GCP field sites thus provides useful insights into the stable isotopic composition of meteoric precipitation in this region.

In total, 28 samples were collected in 2-ml volume glass vials with plastic screw cap. Where possible, vials were filled completely to the top so that no air bubbles remained. As far as was possible, samples were stored in a cool environment or refrigerated at c.4°C until analysis.

Samples were analyzed for isotopic composition using a Picarro L2140-i CRDS instrument. Analytical precision is better than 0.1 and 0.05‰ for $\delta^{18}O$ and δD (1σ), respectively. Standardization was accomplished using VSMOW, Greenland Ice Sheet Project 2 (GISP2), and Standard Light Antarctic Precipitation (SLAP) reference solutions. Results are shown in Fig. 8 and table S2.

SUPPLEMENTARY MATERIALS

Supplementary material for this article is available at http://advances.sciencemag.org/cgi/content/full/7/13/eabe1260/DC1

REFERENCES AND NOTES

1. Past Interglacials Working Group of PAGES, Interglacials of the last 800,000 years. *Rev. Geophys.* **54**, 162–219 (2016).
2. Q. Z. Yin, A. Berger, Insolation and CO_2 contribution to the interglacial climate before and after the Mid-Brunhes Event. *Nat. Geosci.* **3**, 243–246 (2010).
3. Q. Z. Yin, A. Berger, Individual contribution of insolation and CO_2 to the interglacial climates of the past 800,000 years. *Climate Dynam.* **38**, 709–724 (2012).
4. J. H. F. Jansen, A. Kuijpers, S. R. Troelstra, A Mid-Brunhes climatic event: Long term changes in global atmosphere and ocean circulation. *Science* **232**, 619–622 (1986).
5. P. Wang, J. Tian, X. Cheng, C. Liu, J. Xu, Carbon reservoir changes preceded major ice-sheet expansion at the Mid-Brunhes Event. *Geology* **31**, 239–242 (2003).
6. P. C. Tzedakis, D. Raynouad, J. F. McManus, A. Berger, V. Brovkin, T. Kiefer, Interglacial diversity. *Nat. Geosci.* **2**, 751–755 (2009).
7. EPICA Community Members, Eight glacial cycles from an Antarctic ice core. *Nature* **429**, 623–628 (2004).
8. I. Candy, G. R. Coope, J. R. Lee, S. A. Parfitt, R. C. Preece, J. Rose, D. C. Schreve, Pronounced warmth during early Middle Pleistocene interglacials: Investigating the Mid-Brunhes Event in the British terrestrial sequence. *Earth Sci. Rev.* **103**, 183–196 (2010).

9. A. A. Prokopenko, L. A. Hinnov, D. F. Williams, M. I. Kuzmin, Orbital forcing of continental climate during the Pleistocene: A complete astronomically tuned climatic record from Lake Baikal, SE Siberia. *Quat. Sci. Rev.* **25**, 3431–3457 (2006).
10. J. A. Snyder, M. V. Cherepanaova, A. Bryan, Dynamic diatom response to changing climate 0-1.2 Ma at Lake El'gygytgyn, Far East Russian Arctic. *Clim. Past* **9**, 1309–1319 (2013).
11. E. Willerslev, E. Cappellini, W. Boomsma, R. Nielsen, M. B. Hebsgaard, T. B. Brand, M. Hofreiter, M. Bunce, H. N. Poinar, D. Dahl-Jensen, S. Johnsen, J. P. Steffensen, O. Bennike, J.-L. Schwenninger, R. Nathan, S. Armitage, C.-J. de Hoog, V. Alfimov, M. Christl, J. Beer, R. Muscheler, J. Barker, M. Sharp, K. E. H. Penkman, J. Haile, P. Taberlet, M. T. P. Gilbert, A. Casoli, E. Campani, M. J. Collins, Ancient biomolecules from deep ice cores reveal a forested southern Greenland. *Science* **317**, 111–114 (2007).
12. D. Veres, L. Bazin, A. Landais, H. T. M. Kele, B. Lemieux-Dudon, F. Parrenin, P. Martinerie, E. Blayo, T. Blunier, E. Capron, J. Chappellaz, S. O. Rasmussen, M. Severi, A. Svensson, B. Vinther, E. W. Wolff, The Antarctic ice core chronology (AICC2012): An optimized multi-parameter and multi-site dating approach for the last 120 thousand years. *Clim. Past* **9**, 1733–1748 (2013).
13. L. Bazin, A. Landais, B. Lemieux-Dudon, H. T. M. Kele, D. Veres, F. Parrenin, P. Martinerie, C. Ritz, E. Capron, V. Lipenkov, M.-F. Loutre, D. Raynaud, B. Vinther, A. Svensson, S. O. Rasmussen, M. Severi, T. Blunier, M. Leuenberger, H. Fischer, V. Masson-Delmotte, J. Chappellaz, E. W. Wolff, An optimized multi-proxy, multi-site Antarctic ice and gas orbital chronology (AICC2012): 120–800 ka. *Clim. Past* **9**, 1715–1731 (2013).
14. D. Lüthi, M. L. Floch, B. Bereiter, T. Blunier, J.-M. Barnola, U. Siegenthaler, D. Raynaud, J. Jouzel, H. Fischer, K. Kawamura, T. F. Stocker, High-resolution carbon dioxide concentration record 650 000–800 000 years before present. *Nature* **453**, 379–382 (2008).
15. L. Loulergue, A. Schilt, R. Spahni, V. Masson-Delmotte, T. Blunier, B. Lemieux, J.-M. Barnola, D. Raynaud, T.-F. Stocker, J. Chappellaz, Orbital and millennial-scale features of atmospheric CH_4 over the past 800 000 years. *Nature* **453**, 383–386 (2008).
16. Arctic Monitoring and Assessment Programme (AMAP), *Snow, Water, Ice and Permafrost Assessment (SWIPA) for the Arctic. Summary for Policy Makers* (AMAP, 2017).
17. T. G. Shepherd, Effects of a warming Arctic. *Science* **353**, 989–999 (2016).
18. R. Bintanja, E. C. van der Linden, The changing seasonal climate in the Arctic. *Sci. Rep.* **3**, 1556 (2013).
19. R. Bintanja, F. M. Selten, Future increases in Arctic precipitation linked to local evaporation and sea-ice retreat. *Nature* **509**, 479–482 (2014).
20. R. Bintanja, O. Andry, Towards a rain dominated Arctic. *Nat. Clim. Change* **7**, 263–267 (2017).
21. M. P. Smith, J. A. Rasmussen, The geology of the Centrumsø area of Kronprins Christian Land, northeast Greenland, and lithological constraints on speleogenesis. *Cave Karst Sci.* **47**, 60–65 (2020).
22. W. E. Davies, D. B. Krinsley, Caves in Northern Greenland. *NSS Bull.* **22**, 114–116 (1960).
23. G. E. Moseley, H. A. Barton, C. Spötl, P. Töchterle, S. E. Bjerkenås, C. Blakeley, P. D. Hodkinson, R. C. Shone, M. P. Smith, M. Wright, Cave discoveries and speleogenetic features in northeast Greenland. *Cave Karst Sci.* **47**, 74–87 (2020).
24. L. Schuster, F. Maussion, L. Langhamer, G. E. Moseley, Lagrangian detection of precipitation moisture sources for an arid region in northeast Greenland: Relations to the North Atlantic Oscillation, sea ice cover and temporal trends from 1979 to 2017. *Weather Clim. Dynam.* **2**, 1–17 (2021).
25. R. S. Fausto, D. van As, Programme for monitoring of the Greenland ice sheet (PROMICE): Automatic weather station data. Version: v03, Dataset published via Geological Survey of Denmark and Greenland (2019).
26. IAEA/WMO, *Global Network of Isotopes in Precipitation. The GNIP Database* (IAEA/WMO, 2020).
27. A. Donner, P. Töchterle, P. G. E. Moseley, Basic meteorological observations in the Centrumsø region of northeast Greenland. *Cave Karst Sci.* **47**, 104–106 (2020).
28. G. E. Moseley, *Northeast Greenland Caves Project Expedition* (Greenland Caves Project, 2016).
29. H. A. Barton, G. J. Breley, P. Töchterle, G. E. Moseley, Cryogenic features of the permafrost ice caves of Grottedal, northeast Greenland. *Cave Karst Sci.* **47**, 93–99 (2020).
30. T. M. L. Wigley, M. C. Brown, in *The Science of Speleology*, T. D. Ford, C. M. D. Cullingford, Eds. (Academic Press, 1976), pp. 329–358.
31. C. H. Hendy, The isotopic geochemistry of speleothems––I. The calculations of the effects of different modes of formation on the isotopic composition of speleothems and their applicability as paleoclimate indicators. *Geochim. Cosmochim. Acta* **35**, 801–824 (1971).
32. A. Berger, Long-term variations of daily insolation and Quaternary climate changes. *J. Atmos. Sci.* **35**, 2362–2367 (1978).
33. H. Cheng, R. L. Edwards, A. Sinha, C. Spötl, L. Yi, S. Chen, M. Kelly, G. Kathayat, X. Wang, X. Li, X. Kong, Y. Wang, Y. Ning, H. Zhang *et al.*, *Nature* **534**, 640–646 (2016).
34. S. Barker, G. Knorr, R. L. Edwards, F. Parrenin, A. E. Putnam, L. C. Skinner, E. Wolff, M. Ziegler, 800,000 years of abrupt climate variability. *Science* **334**, 347–351 (2011).
35. P. Hughes, P. Gibbard, J. Ehlers, The "missing glaciations" of the Middle Pleistocene. *Quatern. Res.* **96**, 161–183 (2020).
36. A. Vaks, A. J. Mason, S. F. M. Breitenbach, A. M. Kononov, A. V. Osinev, M. Rosensaft, A. Borshevsky, O. S. Gutareva, G. M. Henderson, Palaeoclimate evidence of vulnerable permafrost during times of low sea ice. *Nature* **577**, 221–225 (2020).
37. A. de Vernal, C. Hillaire-Marcel, Natural variability of Greenland climate, vegetation, and ice volume during the past million years. *Science* **320**, 1622–1625 (2008).
38. N. Irvali, E. V. Galaasen, U. S. Ninnemann, Y. Rosenthal, A. Born, H. F. Kleiven, A low climate threshold for south Greenland Ice Sheet demise during the late Pleistocene. *Proc. Natl. Acad. Sci. U.S.A.* **117**, 190–195 (2020).
39. T. M. Cronin, G. S. Dwyer, E. K. Caverly, J. Farmer, L. H. DeNinno, J. Rodriguez-Lazaro, L. Gemery, Enhanced Arctic amplification began at the Mid-Brunhes Event ~400,000 years ago. *Sci. Rep.* **7**, 14475 (2017).
40. F. Lambert, B. Delmonte, J. R. Petit, M. Bigler, P. R. Kaufmann, M. A. Hutterli, T. F. Stocker, U. Ruth, J. P. Steffensen, V. Maggi, Dust-climate couplings over the past 800,000 years from the EPICA Dome C ice core. *Nature* **452**, 616–619 (2008).
41. L. E. Lisiecki, M. E. Raymo, A Pliocene-Pleistocene stack of 57 globally distributed benthic $\delta^{18}O$ records. *Paleoceanography* **20**, PA1003 (2005).
42. R. M. Spratt, L. E. Lisiecki, A Late Pleistocene sea level stack. *Clim. Past* **12**, 1079–1092 (2016).
43. Q. Hao, L. Wang, F. Oldfield, G. Zhengtang, Extra-long interglacial in Northern Hemisphere during MISs 15-13 arising from limited extent of Arctic ice sheets in glacial MIS 14. *Sci. Rep.* **5**, 12103 (2015).
44. J. D. Shakun, D. W. Lea, L. E. Lisiecki, M. E. Raymo, An 800-kyr record of global surface ocean $\delta^{18}O$ and implications for ice volume-temperature coupling. *Earth Planet. Sci. Lett.* **426**, 58–68 (2015).
45. A. K. Wright, B. P. Flower, Surface and deep ocean circulation in the subpolar North Atlantic during the mid-Pleistocene revolution. *Paleoceanography* **17**, 1068 (2002).
46. M. Alonso-Garcia, F. J. Sierro, M. Kucera, J. A. Flores, I. Cacho, N. Andersen, Ocean circulation, ice sheet growth and interhemispheric coupling of millennial climate variability during the mid-Pleistocene (ca 800–400 ka). *Quat. Sci. Rev.* **30**, 3234–3247 (2011).
47. N. S. Lord, M. Crucifix, D. J. Lunt, M. C. Thorne, N. Bounceur, H. Dowsett, C. L. O'Brien, A. Ridgwell, Emulation of long-term changes in global climate: Application to the late Pliocene and future. *Clim. Past* **13**, 1539–1571 (2017).
48. B. Lauriol, L. Carrier, P. Thibaudeau, Topoclimatic zones and ice dynamics in the caves of the northern Yukon, Canada. *Arctic* **41**, 215–220 (1988).
49. A. Landais, V. Masson-Delmotte, E. Capron, P. M. Langebroek, P. Bakker, E. J. Stone, N. Merz, C. C. Raible, H. Fischer, A. Orsi, F. Prié, B. Vinther, D. Dahl-Jensen, How warm was Greenland during the last interglacial period? *Clim. Past* **12**, 1933–1948 (2016).
50. NEEM community members, Eemian interglacial re-constructed from a Greenland folded ice core. *Nature* **493**, 489–494 (2013).
51. J. S. Singarayer, P. J. Valdes, High-latitude climate sensitivity to ice-sheet forcing over the last 120 kyr. *Quat. Sci. Rev.* **29**, 43–55 (2010).
52. W. R. Peltier, Global glacial isostasy and the surface of the ice-age earth: The ICE-5G (VM2) model and grace. *Annu. Rev. Earth Planet. Sci.* **32**, 111–149 (2004).
53. K. Fleming, K. Lambeck, Constraints on the Greenland Ice Sheet since the Last Glacial Maximum from sea-level observations and glacial-rebound models. *Quat. Sci. Rev.* **23**, 1053–1077 (2004).
54. A. Lemark, thesis, Niels Bohr Institute Copenhagen University (2010).
55. I. Friedman, J. R. O'Neil, Compilation of stable isotope fractionation factors of geochemical interest, in *Data of Geochemistry*, M. Fleischer Ed. (U. S. Geol. Survey Prof. Paper 440-KK, ed. 6, 1977), pp.1–12.
56. S.-T. Kim, J. R. O'Neil, Equilibrium and non equilibrium oxygen isotope effects in synthetic carbonates. *Geochim. Cosmochim. Acta* **61**, 3461–3475 (1997).
57. D. M. Tremaine, P. N. Froehlich, Y. Wang, Speleothem calcite farmed *in situ*: Modern calibration of $\delta^{18}O$ and $\delta^{13}C$ paleoclimate proxies in a continuously-monitored natural cave system. *Geochim. Cosmochim. Acta* **75**, 4929–4950 (2011).
58. J. Sjolte, G. Hoffmann, S. J. Johnsen, B. M. Vinther, V. Masson-Delmonte, C. Sturm, Modeling the water isotopes in Greenland precipitation 1959-2001 with the meso-scale model REMO-iso. *J. Geophys. Res.* **116**, D18105 (2011).
59. J. Knies, J. Matthiessen, A. Mackensen, R. Stein, C. Vogt, T. Frederichs, S.-I. Nam, Effects of Arctic freshwater forcing on thermohaline circulation during the Pleistocene. *Geology* **35**, 1075–1078 (2007).
60. R. L. Edwards, J. H. Chen, G. J. Wasserburg, ^{238}U–^{234}U–^{230}Th–^{232}Th systematics and the precise measurement of time over the past 500,000 years. *Earth Planet Sci. Lett.* **81**, 175–192 (1987).
61. C.-C. Shen, C.-C. Wu, H. Cheng, R. L. Edwards, Y.-T. Hsieh, S. Gallet, C.-C. Chang, T.-Y. Li, D. D. Lam, A. Kano, M. Hori, C. Spötl, High-precision and high resolution carbonate ^{230}Th dating by MC-ICP-MS with SEM protocols. *Geochim. Cosmochim. Acta* **99**, 71–86 (2012).

62. C. Spötl, Long-term performance of the Gasbench isotope ratio mass spectrometry system for the stable isotope analysis of carbonate microsamples. *Rapid Commun. Mass Spectrom.* **25**, 1683–1685 (2011).
63. D. Scholz, D. L. Hoffmann, StalAge—An algorithm designed for construction of speleothem age models. *Quat. Geochron.* **6**, 369–382 (2011).
64. P. J. Valdes, E. Armstrong, M. P. S. Badger, C. D. Bradshaw, F. Bragg, M. Crucifix, T. Davies-Barnard, J. J. Day, A. Farnsworth, C. Gordon, P. O. Hopcroft, A. T. Kennedy, N. S. Lord, D. J. Lunt, A. Marzocchi, L. M. Parry, V. Pope, W. H. G. Roberts, E. J. Stone, G. J. L. Tourte, J. H. T. Williams, The BRIDGE HadCM3 family of climate models: HadCM3@ Bristol v1.0. *Geosci. Model Dev.* **10**, 3715–3743 (2017).
65. J. Laskar, P. Robutel, F. Joutel, M. Gastineau, A. C. M. Correia, B. Levrard, A long-term numerical solution for the insolation quantities of the Earth. *Astronomy Astrophysics* **428**, 261–285 (2004).
66. B. Bereiter, S. Eggleston, J. Schmitt, C. Nehrbass-Ahles, T. F. Stocker, H. Fischer, S. Kipfstuhl, J. Chappellaz, Revision of the EPICA Dome C CO_2 record from 800 to 600 kyr before present. *Geophys. Res. Lett.* **42**, 542–549 (2015).
67. L. B. Stap, R. S. W. Van De Wal, B. De Boer, R. Bintanja, L. J. Lourens, The influence of ice sheets on temperature during the past 38 million years inferred from a one dimensional ice sheet-climate model. *Clim. Past* **13**, 1243–1257 (2017).
68. G. E. Moseley, History of exploration in northeast Greenland. *Cave Karst Sci.* **42**, 55–59 (2020).
69. I. Joughin, B. Smith, I. Howat, T. Moon, T. Scambos, A SAR record of early 21st century change in Greenland. *J. Glaciol.* **62**, 62–71 (2016).
70. U.S. National Ice Center and National Snow and Ice Data Center. Compiled by F. Fetterer, M. Savoie, S. Helfrich, P. Clemente-Colón. 2010, updated daily. "Multisensor Analyzed Sea Ice Extent—Northern Hemisphere (MASIE-NH), Version 1" (2002).
71. J. Obu, S. Westermann, A. Kääb, A. Bartsch, *Ground Temperature Map, 2000–2016, Northern Hemisphere Permafrost* (Alfred Wegener Institute, Helmholtz Centre for Polar and Marine Research, 2018).
72. © EuroGeographics. Original product is freely available at eurogeoarchive.srgry.uk. Terms of the license available at https://eurogeographics.org/maps-for-europe/open-data/topographic-data/.
73. A. Berger, M. F. Loutre, Insolation values for the climate of the last 10 million years. *Quat. Sci. Rev.* **10**, 297–317 (1991).
74. E. W. Wolff, J. Chappellaz, T. Blunier, S. O. Rasmussen, A. Svensson, Millennial-scale variability during the last glacial: The ice core record. *Quat. Sci. Rev.* **29**, 2828–2838 (2010).
75. H. Cheng, R. L. Edwards, C.-C. Shen, V. J. Polyak, Y. Asmerom, J. Woodhead, J. Hellstrom, Y. Wang, X. Kong, C. Spötl, X. Wang, E. Calvin Alexander Jr., Improvements in ^{230}Th dating, ^{230}Th and ^{234}U half-life values, and U–Th isotopic measurements by multi-collector inductively coupled plasma mass spectrometry. *Earth Planet. Sci. Lett.* **371–372**, 82–91 (2013).
76. A. H. Jaffey, K. F. Flynn, L. E. Glendenin, W. C. Bently, A. M. Essling, Precision measurement of half-lives and specific activities of ^{235}U and ^{238}U. *Phys. Rev. C* **4**, 1889 (1979).
77. K. H. Wedepohl, The composition of the continental crust. *Geochim. Cosmochim. Acta* **59**, 1217–1232 (1995).

Acknowledgments: We thank C. Blakeley, R. Shone, and M. Wright for assistance in the field; C. Johnson, J.-F. Loubiere, P. Smith, Cambridge Arctic Shelf Programme, Mestersvig personnel, and Norlandair for logistical assistance; and M. Wimmer, J. Degenfelder, Y. Lu, S. Carolin, T. Philipp, and K. Gröbner for analytical support and manuscript development. **Funding:** This work was supported by funding from the Austrian Science Fund (project numbers T 710-NBL and Y 1162-N37) to G.E.M. and by funding from the U.S. NSF (grant 1702816 to R.L.E.). N.S.L. was supported by EMERGENCE (NE/S005242/1). H.C. was supported by NSFC 41888101. In addition, the fieldwork was funded and supported by the National Geographic Society (9638-15); University of Innsbruck Nachwuchsförderung (NWF2014/GEO13); Comer Family Foundation (CP108); Petzl Foundation; P. and L. Shone; Innsbruck Quaternary Research Group; Go Balance; G. E. Moseley; Mount Everest Foundation (15-04); Austrian Academy of Sciences; British Cave Research Association; Transglobe Expedition Trust; R. C. Shone; S. and P. Moseley; National Speleological Society; Quaternary Research Association; Wilderness Lectures; Ghar Parau Foundation (GPF2014b-002); BBC Radio 3 Speaker's Fee; Chris Blakeley; Limestone Research and Consultancy Ltd.; A. Eavis; Lake Fellowship of Unitarian Universalists; T. Arbenz Netopyr Products; I. Fairchild; D. Gibson; G. Hawkins; L. Nicholson; Easyfundraising; R. Dowling; H. and A. Carson; J. Vetterlein; A. Hinkle; S. Brandstätter; K. Newton; M. Higgins; J. Wade; T. Faulkner; C. and J. Leech; C. Spötl; M. Wright; P. Ellingson; A. Fayon; Gouffre Berger Book Project; Bellroy; FIA Formula E Championship; J. Immen; Hilti Austria; Ortlieb; Red Bull; Petzl, Scanlico Denmark; Suunto; Swarovski Optik; Virgin Balloon Flights; and Voltaic Systems. **Author contributions:** G.E.M.: conceptualization, methodology, validation, formal analysis, and investigation, writing (original draft), writing (review and editing), visualization, project administration, and funding acquisition. R.L.E.: resources, writing (review and editing), and funding acquisition. N.S.L.: methodology, software, validation, formal analysis, investigation, writing (review and editing), and visualization. C.S.: resources, writing (review and editing), and funding acquisition. H.C.: writing (review and editing) and funding acquisition. **Competing interests:** The authors declare that they have no competing interests. **Data and materials availability:** All data needed to evaluate the conclusions in the paper are present in the paper and/or the Supplementary Materials. Additional data related to this paper may be requested from the authors. This product includes Intellectual Property from European National Mapping and Cadastral Authorities and is licensed on behalf of these by EuroGeographics. Original product is freely available at eurogeoarchive.srgry.uk. Terms of the license are available at http://eurogeoarchive.srgry.uk/form/topographic-data-eurogeographics. Short form—© EuroGeographics. Original product is freely available at eurogeoarchive.srgry.uk. Terms of the license are available at http://eurogeoarchive.srgry.uk/form/topographic-data-eurogeographics.

Submitted 1 August 2020
Accepted 9 February 2021
Published 24 March 2021
10.1126/sciadv.abe1260

Citation: G. E. Moseley, R. L. Edwards, N. S. Lord, C. Spötl, H. Cheng, Speleothem record of mild and wet mid-Pleistocene climate in northeast Greenland. *Sci. Adv.* **7**, eabe1260 (2021).